Nuclear Stopping in Mass Asymmetric Nuclear Collisions due to Isospin Momentum Dependent Interactions

Dissertation submitted for the partial fulfillment of requirement for
The award of the degree of

Master of Science
In
Physics

Submitted by
Prachi Gautam
Roll no. 301204006

Under the guidance of
Dr. Suneel Kumar

School of Physics and Material Science
Thapar University
Patiala – 147004 (PUNJAB), INDIA

CERTIFICATE

I hereby declare that the report entitled "Nuclear Stopping in Mass Asymmetric Nuclear Collisions due to Isospin Momentum Dependent Interactions" is an authentic record of my own work carried out for the partial fulfillment of the award of the degree of Masters of Science in Physics at Thapar University, Patiala (Punjab), under the guidance of Dr. Suneel Kumar, Associate Professor, School of Physics and Materials Sciences, Thapar University, Patiala. The matter presented in the dissertation has not been submitted in part or full for the award of any other degree.

Prachi

Date: 10/07/2014

Prachi Gautam
Roll No. : 301204006

It is certified that the above statement made by the candidate is correct to the best of my knowledge and belief.

S Kumar

(Dr. Suneel Kumar)

Associate Professor
School of Physics and Materials Science
Thapar University, Patiala

(Dr. Kulvir Singh)

Professor
Head
School of Physics and Materials Science
Thapar University, Patiala

(Dr. S.K. Mohapatra)

Senior Professor
Dean of Academic Affairs
Thapar University, Patiala

ACNOWLEDGEMENT

One looks back with appreciation to the brilliant teachers, but with gratitude to those who touched our human feelings. The curriculum is so much necessary raw material, but warmth is the vital element for the growing plant and for the soul of the child.

— Carl Jung

The writing of this dissertation has been one of the most significant academic challenges I have ever had to face. During this period I have been blessed by Almighty with some extraordinary people who have spun a web of support around me. I would like an attempt to thank them for making my time during my work in the Institute a period I will treasure.

I am deeply indebted to my research supervisor, ***Dr. Suneel Kumar*** *for his guidance, professional supervision and encouragement. His wisdom, knowledge and commitment to the highest standards inspired and motivated me. He was the best choice I could have made for an advisor. Sometime we are just (or incredibly) lucky!!!*

I would like to thank ***Dr. Kulvir Singh****, Head, School of Physics and Material Science for his support for providing me the necessary lab facilities.*

A hearty thanks to ***Ms. Navjot Kaur Virk*** *for her continuous support, proposed ideas, valuable discussions and constructive suggestions. Her cooperation, positive attitude and understanding really deserve an everlasting appreciation. I could not imagine completing my dissertation successfully without her. My sincere thanks to all the research scholars of the physics department for their help and valuable suggestions.*

Last but not the least, I would like to thank my family for their support and unconditional love. Even though we are hundreds of miles away, you were always there whenever I needed you. You can take all the credit for much of what I have achieved and what I will achieve in the future.

I would like to acknowledge the financial support provided by the Department of Atomic Energy (DAE), Government of India, vide sanction No. 2012/37P/16/BRNS.

Prachi

Prachi Gautam
301204006

Date: 10/07/2014

List of Publications:

a. Insensitivity of global nuclear stopping towards isospin effects due to momentum dependent interactions.
Navjot Kaur Virk, Prachi Gautam, and Suneel Kumar
Proc. of 75-years of Nuclear Fission: Present Status and Future Perspectives, May 8-10, 2014, Pg. No. **111**

b. Influence of Isospin Momentum Dependent Interactions on Nuclear Stopping in Mass Asymmetric Nuclear Collisions.
Navjot Kaur Virk, Prachi Gautam, Suneel Kumar, Rajeev Kumar Puri and Sailajananda Bhattacharya (to be submitted)

CONTENTS

Page No.

Chapter 1: Introduction

Chapter 2: Methodology

Chapter 3: Nuclear Stopping

ABSTRACT

In the present study, nuclear stopping has been analyzed for the various mass asymmetric nuclear reactions (fixed target and different projectiles) under the influence of soft-momentum-dependent (SMD) and isospin-soft-momentum dependent (ISMD) interactions. For this, the simulations have been carried out within the framework of Isospin-dependent Quantum Molecular Dynamics (IQMD) model for the reactions ${}^{16}_{8}O+{}^{197}_{79}Au$, ${}^{32}_{16}S+{}^{197}_{79}Au$, ${}^{65}_{30}Zn+{}^{197}_{79}Au$, ${}^{118}_{50}Sn+{}^{197}_{79}Au$, and ${}^{131}_{54}Xe+{}^{197}_{79}Au$ at the different incident energies and over the whole colliding geometry. It has been revealed that the degree of nuclear stopping decreases for heavier charged fragments, and ISMD plays a significant role in the reactions induced by lighter projectile. Also, if one considers the anisotropy ratio due to neutrons and protons separately, ISMD has been found to play a considerable role for the reaction ${}^{131}_{54}Xe + {}^{197}_{79}Au$ in the mid-rapidity region. This motivates one to further investigate the role of ISMD towards the various aspects of heavy ion collisions.

Chapter 1: Introduction

More than 99% of the mass of visible matter in the universe is nuclear matter in which protons and neutrons (nucleons) are the building blocks of atomic nuclei.

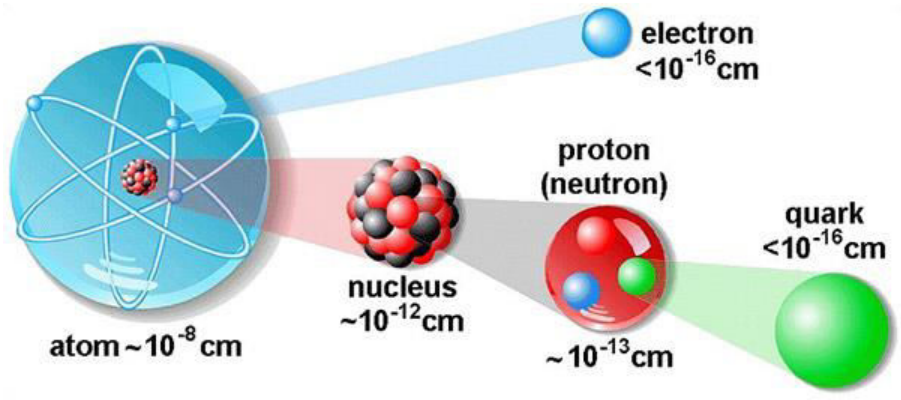

Fig.1.1 Pictorial view of elementary parts of an atom.

Fig.1.1 shows a pictorial view of elementary parts of an atom. Exotic forms of nuclear matter were present in the early universe and continue to exist today in neutron stars. Nuclear matter well away from its ground state can be formed during the collision of two nuclei at high bombarding energies [1]. Since the discovery of nucleus, the properties of nuclear matter in general are under continuous investigations. The finite nuclei are studied in great detail with different experimental techniques. Nuclear physics is the field of physics that studies the structure of nuclei, their formation, stability, and decay. It aims to understand the fundamental nuclear forces in nature, their symmetries, and the resulting complex interactions between protons and neutrons in nuclei and among quarks inside hadrons. Nuclear physicists have changed our world. Ongoing research in nuclear physics is not only unraveling the fundamental questions about matter and energy but also enabling a host of new technologies in materials science, biology, chemistry, medicine, and national security. The properties of compressed nuclear matter became accessible with the development of accelerators with energies beyond the threshold energies for the production of new particles and the capability to accelerate heavy ions, which enables the creation of large volumes of hot and dense nuclear matter. With increase in the incident beam energy, new phenomena can be observed, e.g., the production of the particles which are not present in the entrance channel or the collective properties of the reaction products.

In the last two decades, substantial theoretical and experimental efforts have been directed to the investigation of the modification of the hadron properties in dense and hot matter. This became possible with the development of accelerators which gives the nuclei enough energy to overcome the electrostatic repulsion between them and this has opened up the field of heavy ion collisions (HICs). The field of nuclear physics which studies the HICs is known as heavy ion physics and is discussed in the next section.

1.1. Heavy Ion Physics

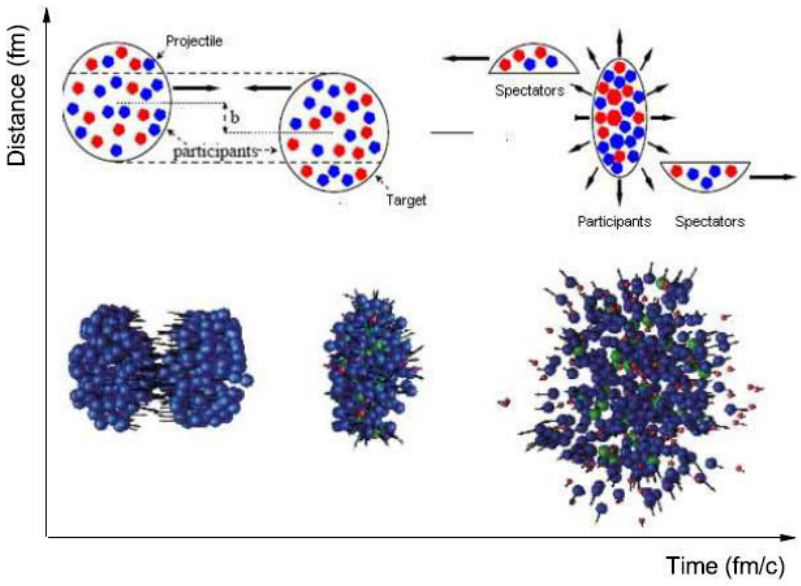

Fig.1.2 Schematic view of a HIC at intermediate energy

The term heavy ion is generally used for the nuclei which are heavier than the helium nucleus [2]. The heavy-ion experiments serves as very important criteria to produce hot and compressed nuclear matter in laboratory as these could serve to determine the nuclear equation of state (EoS) which is related to dependence of the energy per nucleon on the density and temperature [3]. HICs are a unique tool to create and study the hot and dense nuclear matter. Fig.1.2 shows a schematic view of a HIC explaining the impact parameter 'b', participant and spectator zone of the compressed nuclear matter.

On the basis of energy of the two colliding nuclei, HICs can be classified into following three different energy regimes which are explained in detail in the upcoming sections:

- Low energy HICs (E < 10 MeV/nucleon)
- Intermediate energy HICs (10 MeV/nucleon ≤ E ≤ 2 Gev/nucleon)
- High energy HICs (E > 2 GeV/nucleon)

1.1.1 Low Energy HICs

When two nuclei collide at a low energy (i.e. E < 10 MeV/nucleon), the compound nucleus formation takes place which gives rise to various phenomena like fission, fusion, cluster-radioactivity, formation of super heavy elements, halo nuclei, etc.

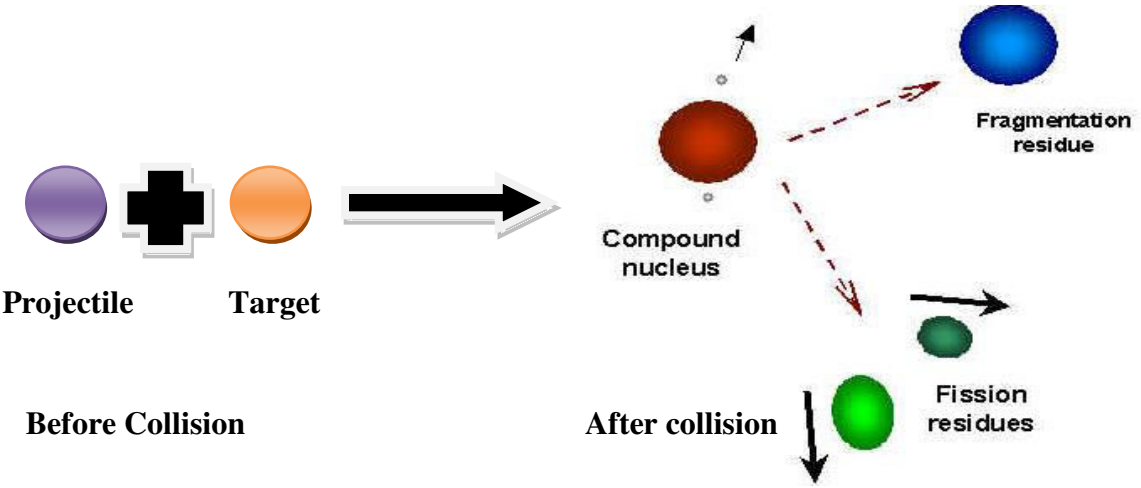

Fig.1.3 Schematic view of HICs at low energy with compound nucleus formation.

The main contribution to the reaction cross section comes from the compound nucleus formation and deep inelastic scattering [4]. The whole dynamics at low energy is governed by the mean field. About 98% of the collisions are blocked due to the lack of available phase space, hence, nucleon-nucleon collisions are negligible. The dominating role of nucleon mean field at low energy produces central fusion and peripheral deep inelastic collisions [5].Fig.1.3 shows a schematic view of a HIC which occurs at low energy, where a compound nucleus is formed, which further results in a fragmentation residue and fission residues.

1.1.2 Intermediate Energy HICs

At intermediate energy, the available phase space is enlarged which results in collisions between the nucleons. Here, both the mean field as well as the nucleon-nucleon collisions are significant. Reactions at this energy regime results in the breaking of the initial correlations between the nucleons, but not enough to break their internal structure. Here, the study the of two body collisions in a limited volume for peripheral collisions (participant-spectator picture) and total volume in central collisions (explosion like collisions) is important. This energy regime is the intervening region and it is therefore, very important to study the energy and mass dissipation here in order to find answers to fundamental questions about the behavior of nuclear matter at high temperature and density reached in HICs [5].

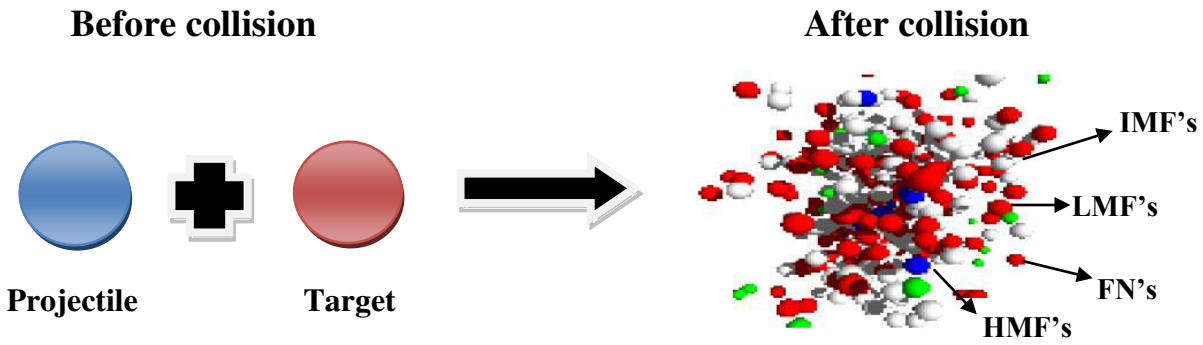

Fig.1.4 Schematic view of HICs at intermediate energies.

Different phenomena like multifragmentation, collective flow and nuclear stopping are being studied at this energy range [6]. Fig.1.4 shows a schematic view of a HIC at intermediate energy, where a projectile nuclei hits a target nuclei that leads to the formation of a compressed matter which further results in the formation of different fragments i.e. free nucleons (FN's) [A=1], light mass fragments (LMF's) [2≤A≤4], intermediate mass fragments (IMF's) [5≤A≤A_{total}/6] and heavy mass fragments (HMF's) [21≤A≤A_{total}/6]. In a HIC at intermediate energy, the density achieved is 2–4 times the normal nuclear matter density (ρ_0 = 0.17 fm^{-3}), where ρ_0 is the normal nuclear matter density and, the temperature is of the order of 100 MeV. The properties of the nuclear matter at high density and temperature are not only of importance for nuclear physicists, but also of great use for the astrophysical studies, especially for supernova studies and for revealing the information regarding the evolution of the universe [7, 8].

1.1.3 High Energy HICs

The HICs at high energy mainly concerns with the fundamental particle production. Fig.1.5 shows a schematic view of a HIC at high energy which results in the formation of fundamental particles which are quarks and leptons. Here, in this energy range, the mean field is negligible, while nucleon-nucleon collision plays a dominant role. The phase space available at high energy is very large, due to which the Pauli blocking role is minimized, i.e., roughly 4% collisions are blocked. At high densities and temperature, there is a transition from hadronic gas phase to quark gluon plasma phase (high energy phase) [8].

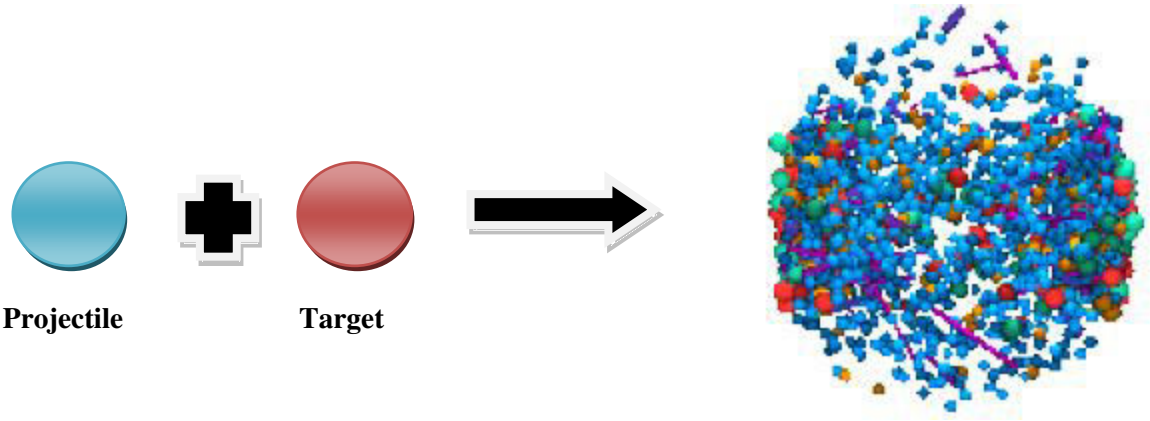

Fig.1.5 Schematic view of a HIC at high energy.

Furthermore, depending upon the size of the colliding nuclei, HICs can be classified into two categories namely (i) Mass Symmetric and, (ii) Mass Asymmetric HICs. However, the main concentration of this work is on Mass Asymmetric HIC, particularly, the one in which the target is kept fixed and the projectile is altered. The next section explains the mass asymmetry.

1.2 Mass Asymmetry

The mass asymmetry of a reaction can be defined by the parameter, where A_T and A_P are the masses of the target and projectile nuclei respectively. The η=0 corresponds to the symmetric reactions, while non-zero value of η corresponds to asymmetric reactions. The reaction dynamics

of a symmetric reaction is quite different from that of an asymmetric reaction at both low and intermediate energies. This difference emerges due to the difference in transfer of energy in symmetric and asymmetric reactions. For more understanding, the phase space and momentum space analysis of $^{16}_{8}\mathrm{O} + {}^{197}_{79}\mathrm{Au}$ (asymmetric reaction, η=0.849) and $^{197}_{79}Au + {}^{197}_{79}Au$ (symmetric reaction, η=0) has been discussed in section 3.4 of chapter 3.

The aim of the present work is to estimate the degree of nuclear stopping in asymmetric HICs. The criterion to choose the mass asymmetric reactions is to take the heavier target and lighter projectile. The next section elaborates the nuclear stopping.

1.3 Nuclear Stopping

It is an important phenomenon which provides the information regarding the equilibrium or thermalization reached in a reaction such that to obtain the idea about the reaction dynamics. The nuclear stopping is defined as the randomization of one-body momentum space or memory loss of the incoming momentum. More the initial memory is lost, better it is stopped. When the two nuclei collide to form a compressed matter, it results in the heating of the matter. The destruction of the initial correlation makes the matter homogeneous and hence one can observe a global stopping. The phenomenon of nuclear stopping originates from the participant zone. The degree of stopping depends on the incident energy, mass of the colliding nuclei (A_T and A_P) and their colliding geometry (b). It can be related to the properties of the system, nuclear EoS and in medium properties of the nucleon-nucleon cross section [9]. Nuclear stopping governs the amount of dissipated energy, the amplitude of large collective motion and the competition between various mechanisms such as deep inelastic reactions, neck emission and fusion reactions [10].

Under some specific conditions when two nuclei collide, three different cases can be observed which are shown in Fig.1.6:

Case 1: Full stopping,

Case 2: Stopping and mixing, and

Case 3: Transparency.

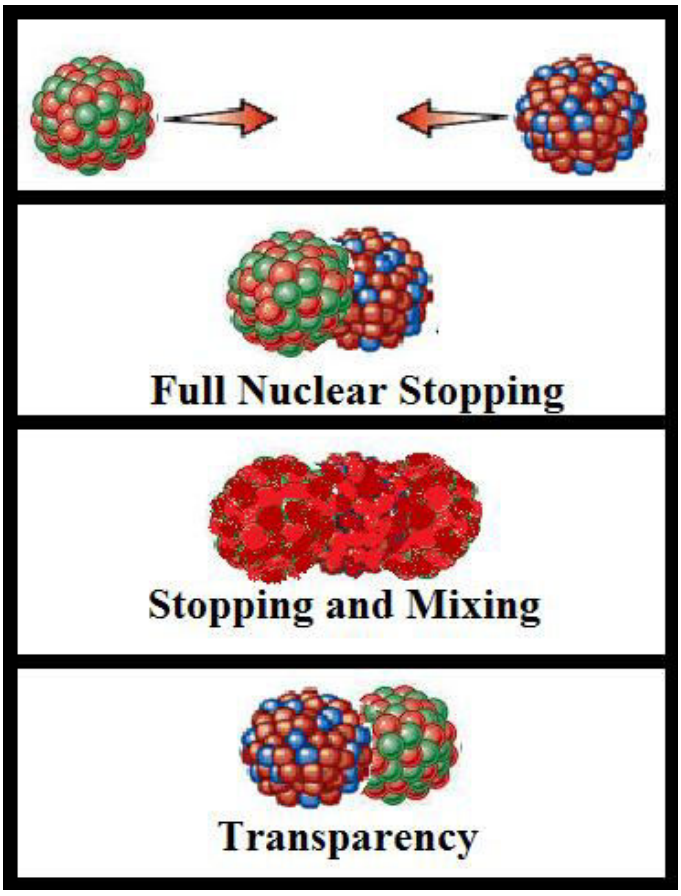

Fig.1.6 Schematic view of nuclear stopping at different energies.

The first figure shows a projectile and a target nuclei heading towards each other. In Case 1 the two nuclei collide, and are repelled by each other such that, they are being fully stopped. Case 2 shows the two nuclei in a compressed form which are being mixed up, like in a collision of two droplets and thus, are termed as stopping and mixing. Case 3 depicts transparency in the collision of two nuclei as they passes through each other without any interaction. This case occurs at high energy.

1.4 Experimental Review

Various experimentalists have contributed significantly for nuclear stopping in intermediate energy HICs. Efforts made by different collaborations have been summarized as follows:

- The FOPI Collaboration [11] studied the nuclear stopping for the various symmetric as well as asymmetric reactions at incident energies of the order of intermediate energies. The observables include cluster multiplicities, longitudinal and transverse rapidity distributions, stopping, and radial flow.
- Another study for global nuclear stopping is performed by Lehaut *et al*. [10], in central collisions at intermediate energies with the help of 4π multi-detector INDRA for a large variety of symmetric and asymmetric reactions.
- The FOPI collaboration studied the degree of equilibration in central HICs using isospin (N/Z) degree of freedom for Ru(Zr)+Zr(Ru) reactions at 400 MeV/A [12].
- In 2003, FOPI Collaboration presented the methods to test the degree of nuclear stopping power by using isospin asymmetric nuclear collisions. The results consistently demonstrate incomplete mixing and partial transparency of the projectile and target nuclei at SIS energies. [13].
- The Berkeley group focuses mainly on the asymmetric reactions at incident energy between 50 and 110 MeV/nucleon. Their aim was to investigate the role of entrance channel mass asymmetry on the reaction dynamics [14].

Besides the above experimental attempts, various theoreticians also discussed the nuclear stopping. The theoretical overview of nuclear stopping is discussed in the forthcoming section.

1.5 Theoretical Review

The phenomenon of nuclear stopping was introduced by Bass *et al*. [15], via the "isospin-mixing" method. In 1998, Li *et al*. [16], found that the degree of isospin equilibrium depends sensitively on both the in-medium NN cross-section and EoS of asymmetric nuclear matter. In 2002, R.K. Puri *et al*. [17], studied the possibility of equilibrium in HICs at intermediate energies within a transport model by taking various symmetric and asymmetric reactions. They found that nucleons that suffer at least 10 collisions are close to complete equilibrium, whereas the others never achieve any equilibrium. In 2004, T. Gaitanos *et al*. [18], analyzed the stopping and isospin equilibration in relativistic collisions in terms of the imbalance ratio of different particle types in projectile/target rapidity regions in mixed collisions. In 2010, S. Kumar *et al*. [19], studied the role of symmetry energy with and without momentum dependent interactions (MDI)

on the global nuclear stopping. The nuclear stopping is found to be sensitive towards MDI and symmetry energy at low incident energies. This study reveals that the MDI play an important role towards the nuclear stopping. In 2011, A.D. Sood *et al*. [20], obtained the information about the thermalisation and stopping in HICs via relative momentum, anisotropy ratio and rapidity distribution for nearly symmetric and asymmetric systems. In 2011, V. Kaur *et al*. [21], analyzed the nuclear stopping in asymmetric colliding channels by keeping the total mass fixed. They found the effect of mass asymmetry on nuclear stopping and on equilibrium of the nuclear matter at an incident beam energy of 250 MeV/nucleon. In 2013, E. Bonnet *et al*. [22], studied stopping for asymmetric reaction Xe + Sn. It has been seen that LCP's are considered to be better indicator for nuclear stopping because they behave in similar fashion as that of anisotropy ratio [23].

Most of the above mentioned theoretical and experimental studies concentrated more on the dynamics for symmetric reacting partners than for asymmetric systems. We here, in this thesis, plan to work for asymmetric systems in which the target mass is kept fixed and projectile mass is varied and will discuss the effect of isospin-momentum dependent interaction (IMDI) on the nuclear stopping taking parameter as anisotropic ratio R (will be discussed in chapter 3).

To achieve this aim, isospin dependent quantum molecular dynamic model (IQMD) [24] and its IQMD (Th01) [25] version is used. Before moving to the results, the primary and secondary models are described in the next chapter.

Chapter 2: Methodology

2.1 Review of Various Theoretical Models

In the last few decades, major efforts were made to develop the microscopic models which can describe the dynamics of HICs at intermediate energies. The numerical modelling of HICs involve very complicated non-equilibrium physics. The theoretical models for the different phenomena taking place at intermediate energies can be divided into two categories namely statistical and dynamical models.

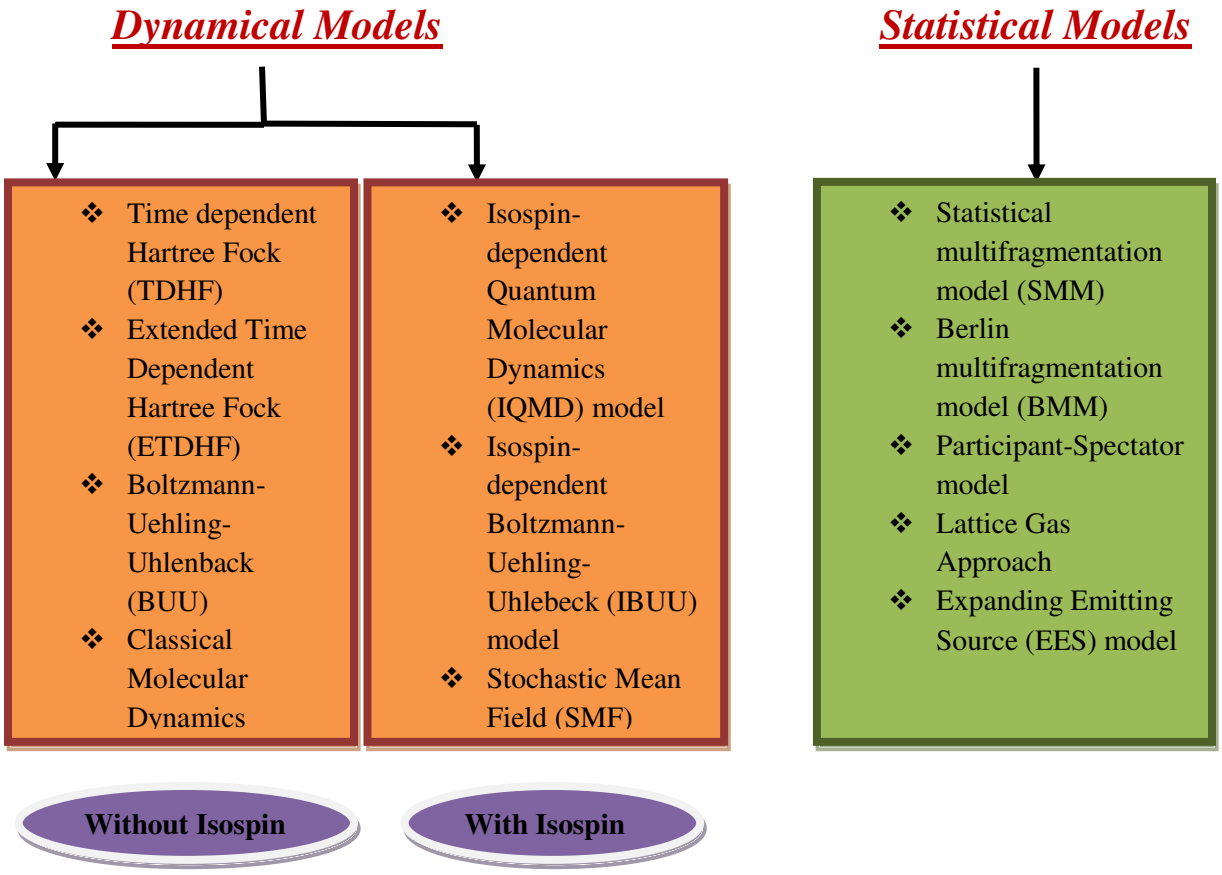

Fig.2.1 Classification of various theoretical models

The statistical models give the information about the initial and final stage of the reaction and does not account for the complete reaction process. Some of the statistical models [26] are

Statistical Multifragmentation model (SMM), Berlin Multifragmentation model (BMM), Participant-Spectator model, etc. The statistical models give a better elucidation of the final stage of the reaction and neglect the dynamics of the collision. Hence, depend on the initial excitation energy and density of the composite system only. Also, in statistical models, the situation at the start of the reaction is based on some assumption for the degree of thermalization. Therefore, in order to study the time evolution of HIC namely: initialization, compression and expansion, statistical models are neglected and dynamical models are preferred. There are various dynamical models such as Time dependent Hartree Fock (TDHF) [27] approximation for the microscopic description of the dynamics of the HIC, where the fermions are assumed to interact only through the mean field while the collisions between them due to residual interactions are neglected. Thus, it is not suitable to study the reaction dynamics at intermediate energy, where the mean field and nucleon-nucleon collisions both plays a vital role. Later on, attempts were made to extend the TDHF to include nucleon-nucleon (NN) collisions which is known as Extended Time Dependent Hartree-Fock (ETDHF) equation, but it could not cope with large scale investigations of HIC due to computation problems. Another model named Boltzmann-Uehling-Uhlenbeck model [28] is able to explain the one body observables namely collective flow, nuclear stopping and particle production, while N-body features like multifragmentation are not described by this model because the correlations and fluctuations were not preserved. Isospin-dependent Boltzmann-Uehling-Uhlembeck (IBUU) model [29] was introduced to study the HICs that include the isospin effects. The isospin dependence enters through nucleon-nucleon cross-section and the nuclear mean field. The Intra Nuclear Cascade (INC) Model [30] is a dynamical model used to understand the experimental data of HICs, but it neglects the mean field, while nucleon-nucleon collisions are taken into account without Pauli blocking, i.e., it is capable of describing the high energy HICs. Aichelin and Stöcker in 1991, incorporated the quantum features like the Pauli principle, stochastic scattering and particle production in a model which is dubbed as Quantum Molecular Dynamics (QMD) model [8].

QMD is a n-body theory which simulates the HICs at intermediate energies on an event-by-event basis, where each event is simulated independent of other events, but, it does not include the isospin factor of the nucleons in it.

Several improvements were made in the QMD model to give new version to it like BQMD, HQMD, RQMD, IQMD, [24] etc. In the present work, we will solely confine ourself to Isospin-

dependent Quantum Molecular Dynamics (IQMD) model and IQMD (Th01) model. Both these models are discussed in detail in the following section.

2.2 IQMD Model

IQMD model is an extension of the QMD model, which incorporates the isospin degree of freedom, i.e., the neutron and proton are now distinguished from each other. It was developed by Hartnack *et al.*, [24]. This model treats different charge states of the nucleons, deltas and pions explicitly. The isospin degree of freedom enters into the calculations via symmetry potential, cross sections and Coulomb interactions. This model includes three steps: firstly, the nuclei have to be generated under certain conditions. This procedure is called as *initialization*. The generated nuclei propagate under the influence of surrounding mean field, termed as *propagation*. Finally, nucleons are bound to collide, if they come too close to each other. This part is dubbed as *collision*. The model has been used successfully for the analysis of large number of observables from low to relativistic energies [22, 31].

2.2.1 Initialization

Each nucleon is represented by a Gaussian-shaped density distribution. The nucleons interact by mutual two and three body forces. The distribution function is defined as:

$$f_i(r,p,t) = \frac{1}{\pi^2\hbar^2}\, e^{-(r-r_i(t))^2\frac{1}{2L}}\, e^{-(p-p_i(t))^2\frac{2L}{\hbar^2}} \quad (1)$$

Here, the Gaussian width 'L' represents the interaction range of the particle. In IQMD model, L varies with the size of the system in order to obtain maximum stability of the nucleonic density profiles. The value of L is 8.66 fm^2 for Au+Au and 4.33 fm^2 for Ca+Ca and lighter nuclei, and in between these two values for the middle mass nuclei.

In accordance with the liquid drop model nucleons are initialized in a sphere with radius $R=1.12A^{1/3}$ fm where the initial momenta are chosen randomly between 0 and Fermi momentum (P_F), without any further local constraints. Here, the Fermi momentum P_F depends on the ground state density. For normal nuclear matter density ρ_0 = 0.17 fm^{-3}, it has a value of 268 MeV/c,

which makes the initialized nuclei less stable. The total N-body function is assumed to be the direct product of coherent states of eqn. (1) and is given as:

$$\phi = \pi_i f_i (r_i, p_i, t) \tag{2}$$

The nucleus is initialized by assigning the co-ordinates and momenta to all nucleons. In three dimensional space (inside a sphere with radius $R = 1.12A^{1/3}$), the centers of Gaussian wave packet r_i are uniformly distributed in polar co-ordinates by

$$\left.\begin{aligned} r &= R\, x_1^{1/3}, \\ cos\theta &= 1 - 2x_2, \\ \phi &= 2\pi x_3, \end{aligned}\right\} \tag{3}$$

where, x_1, x_2 and x_3 are the random numbers. Similarly the center of each Gaussian wave packet p_i is uniformly distributed in polar co-ordinates

$$\left.\begin{aligned} p_i &= p_F (r_i) x_4^{1/3}, \\ cos\theta &= 1 - 2x_5 \ , \\ \phi &= 2\pi x_6. \end{aligned}\right\} \tag{4}$$

where, x_4, x_5 and x_6 are again the random numbers. Typically, only 1 out of 50,000 initializations is accepted under the present criteria. The accepted configurations are quite stable.

2.2.2 Propagation

Nuclei which have been successfully initialized are then boosted towards each other with proper center-of-mass velocity using relativistic kinematics. The nucleons of target and projectile interact via two and three-body Skyrme forces, Yukawa potential and MDIs. The isospin degree of freedom has been taken into consideration by employing Coulomb interactions and symmetry potential among the protons of colliding target and projectile. The hadrons propagate using Hamilton's equations of motion which is given as:

$$\left.\begin{aligned} \frac{dr_i}{dt} &= \frac{\partial\langle H\rangle}{\partial p_i}; \\ \frac{dp_i}{dt} &= -\frac{\partial\langle H\rangle}{\partial r_i} \end{aligned}\right\} \tag{5}$$

where, $\langle H\rangle = \langle T\rangle + \langle V\rangle$

Here, T= Kinetic Energy and V= Potential Energy.

Now,

$$H = \sum_i \frac{p_i^2}{2m_i} + \sum_i \sum_{j>i} \int f_i(r,p,t) V^{ij}(r',r) \times f_j(r',p',t) dr dr' dp dp' \tag{6}$$

The baryon-baryon potential V^{ij}, in the above relation, reads as:

$$V^{ij}(r'-r) = V^{ij}_{Skyrme} + V^{ij}_{Yukawa} + V^{ij}_{Coul} + V^{ij}_{MDI} + V^{ij}_{Sym} \tag{7}$$

Here,

$$V^{ij}_{Skyrme} = \frac{1}{2!}\sum_{j;i\neq j} V^{ij}_{(2)} + \frac{1}{3!}\sum_{j,k;i\neq j\neq k} V^{ijk}_{(3)} \quad , \tag{7a}$$

$$V^{ij}_{Yukawa} = \sum_{j;i\neq j} t_3 \frac{\exp\{-|r_i-r_j|\}/\mu)}{(|r_i-r_j|/\mu)} , \tag{7b}$$

$$V^{ij}_{Coul} = \sum_{j;i\neq j} \frac{Z_i Z_j e^2}{|r_i-r_j|} , \tag{7c}$$

$$V^{ij}_{MDI} = t_4 ln^2\left[t_5\left(p_i-p_j\right)^2+1\right]\left(r_i-r_j\right) \ , \tag{7d}$$

and, $$V^{ij}_{Sym} = t_6 \frac{1}{\varrho_0} T_3^i T_3^j \delta\left(r_i-r_j\right) . \tag{7e}$$

Here, in eq. (7a), $V^{ij}_{(2)}$ and $V^{ijk}_{(3)}$ represents, respectively, the two and three body interactions. The parameter μ and t_1... t_6 are adjusted to the real part of the nucleonic optical potential [24]. In eq. (7d), t_4 = 1.57 MeV and t_5 = 5×10^{-4} MeV^{-2}. In eq. (7c), Z_i and Z_j are the charges of the ith and jth particle respectively, whereas in eq. (7e), T_3^i and T_3^j are their respective T_3 components (i.e.,

1/2 for protons and -1/2 for neutrons). The potentials V_{Yukawa}^{ij} , V_{Skyrme}^{ij} and V_{MDI}^{ij} are isospin independent. The MDI will be discussed in detail in chapter 3. To include the isospin dependence in Coulomb potential real charge is used i.e. $Z_{proton} = 1$ and $Z_{nuetron} = 0$. The Yukawa potential V_{Yuk}^{ij} is very short ranged and weak, where, $\mu = 0.4$ fm. The two body part $V_{(2)}^{ij}$ is directly proportional to $\left(\frac{\rho}{\rho_0}\right)$, whereas, the three body part $V_{(3)}^{ijk}$ is proportional to $\left(\frac{\rho}{\rho_0}\right)^2$. In nuclear matter, the generalized form of the local potential energy has the form,

$$V_{Skyrme} = \frac{\alpha}{2}\left(\frac{\rho}{\rho_0}\right) + \frac{\beta}{\gamma+1}\left(\frac{\rho}{\rho_0}\right)^{\gamma} \tag{8}$$

The above potential has two free (α and β) parameters, which can be fixed by the requirement that at normal nuclear matter density, the average binding energy should be -16 MeV/nucleon and the total energy should have a minimum at ρ_0.

Two different EoS have been implemented using this phenomenon, a hard EoS, and a soft EoS having values given in following table:

EoS	K (MeV)	α (MeV)	β (MeV)	γ
Soft	200	-356	303	1.17
Hard	380	124	70.5	2

2.2.3 Collision

During the propagation, two nucleons are supposed to suffer a collision, if the distance between their centroids is fulfilled by the condition

$$d = \left|r_i - r_j\right| \le \sqrt{\frac{\sigma_{tot}}{\pi}}, \sigma_{tot} = \sigma\left(\sqrt{s}, type\right) \tag{9}$$

where 'type' denotes the ingoing collision partners (N-N, N-Δ, N-π,....).

2.2.4 Pauli Blocking

Pauli blocking (of the final state) of baryons is taken into account by checking the phase space densities of the final state. P_1 and P_2 are the final phase space fractions that are occupied by the nucleons which are determined for each of the scattering baryons. The collision is then blocked with probability

$$P_{block} = 1 - (1 - P_1)(1 - P_2) \tag{10}$$

2.2.5 Cross-Section

The total cross-section is the sum of the elastic and all inelastic cross-sections

$$\sigma_{total} = \sigma_{elastic} + \sigma_{in\text{-}elastic} = \sigma_{elastic} + \Sigma_{channel}\, \sigma_{in\text{-}elastic} \tag{11}$$

The elastic and inelastic cross-sections for proton-proton, neutron-neutron as well as for proton-neutron are affected in the presence of isospin degree. The following inelastic reactions might influence the dynamics of the collision and are explicitly taken into account:

$N\,N \rightarrow \Delta\,N$ (hard − delta production)

$\Delta \rightarrow N\,\pi$ (delta decay)

$\Delta\,N \rightarrow N\,N$ (delta absorption)

$N\,\pi \rightarrow \Delta$ (soft − delta production)

2.3 Clusterization Techniques

Once the phase space is generated by the IQMD model, the different particles are clusterized or grouped into the fragments according to various constraints. This could be done through different clusterization techniques. Some of these are explained in the following sub-sections.

2.3.1 Minimum Spanning Tree (MST)

Two nucleons are clubbed together in a fragment if their centroids are closer than a distance d_{min}, [8, 32], which is given as,

$$|r_i - r_j| \leq d_{min} \quad (12)$$

where, r_i and r_j are the spatial positions of both the nucleons. The value of d_{min} can vary between 3-5 fm. The method gives a single large fragment during the early stage of the reaction, where, density is quite high and the interactions among the nucleons are still active.

2.3.2 Minimum Spanning Tree with Momentum Constraint (MSTP)

An improvement to the MST algorithm is made by imposing a constraint on the relative momentum of nucleons in addition to the spatial constraint. The MSTP method [33] puts a restriction on the spatial as well as momentum space of the nucleons. Nucleons will thus form a fragment, if both the following conditions are followed:

$$\left.\begin{aligned} |r_i - r_j| &\leq d_{min} \\ |p_i - p_j| &\leq p_{min} \end{aligned}\right\} \quad (13)$$

This value of cut in the relative momentum of the two nucleons is about the average Fermi momentum of nucleons. The MSTP method abandons the loosely bounded nucleons from the fragment and increases the stability of the fragments by constraining the relative momentum of nucleons.

For the present analysis, MSTP method has been utilized.

Chapter 3: Nuclear Stopping

Before going into the details of the results, it is advisable to understand the details of MDI and its isospin dependence.

3.1 Momentum Dependent Interactions (MDI)

The static EoS cannot describe the HIC adequately. The fate of the reaction depends not only on the density, but also on the relative momentum of the nucleons. The parameterized form of MDI is given as [34]:

$$V_{MDI}^{ij} = t_4 ln^2 \left[t_5 (p_i - p_j)^2 + 1\right](r_i - r_j) \tag{14}$$

The EoS in its standard Skyrme-type parameterization including momentum dependence is given by:

$$U = \alpha \left(\frac{\rho}{\rho_o}\right) + \beta \left(\frac{\rho}{\rho_o}\right)^{\gamma} + \delta ln^2[\epsilon(\Delta p)^2 \ + \ 1] \ (\rho/\rho_o). \tag{15}$$

If nuclear matter is in highly compressed form, the nucleon-nucleon correlations are already broken due to recurrent and violent nucleon-nucleon collisions. However, if the matter is weakly excited, the MDI can have substantial effect. The MDI suppresses the nucleon-nucleon interactions. This happens because during the high density phase of the reaction, the effect of MDI is very strong, the insertion of MDI accelerates the nucleons in the transverse direction leading to the lower density, which further results into fewer nucleon-nucleon collisions. The reason behind the transverse momentum experienced by the nucleons can be explained by taking an example of a HIC in which a projectile and target nuclei collides at intermediate energy. As long as the projectile and target do not overlap, the relative momentum between the interacting nucleons is small, such that MDI do not play an important role. Now, as soon as the nuclei overlap, particles of very large relative momenta are positioned closely in configuration space [Fig.3.1 (a)]. Here, the projectile nucleons 'feel' a very strong repulsive potential due to the neighboring target nucleons and vice-versa. Outside the overlap region, where there is either projectile or target nucleons, the potential is still attractive [Fig.3.1 (b)]. Hence, there is a strong potential gradient perpendicular to the beam direction which causes a strong force that tries to

sweep particles out of the overlap zone quite early during the reaction. This potential gradient transfers an appreciable amount of transverse momentum to the particles. Hence, a finite transverse momentum transfer is seen, which results in the expansion of the system radially, thereby, reducing the density [8].

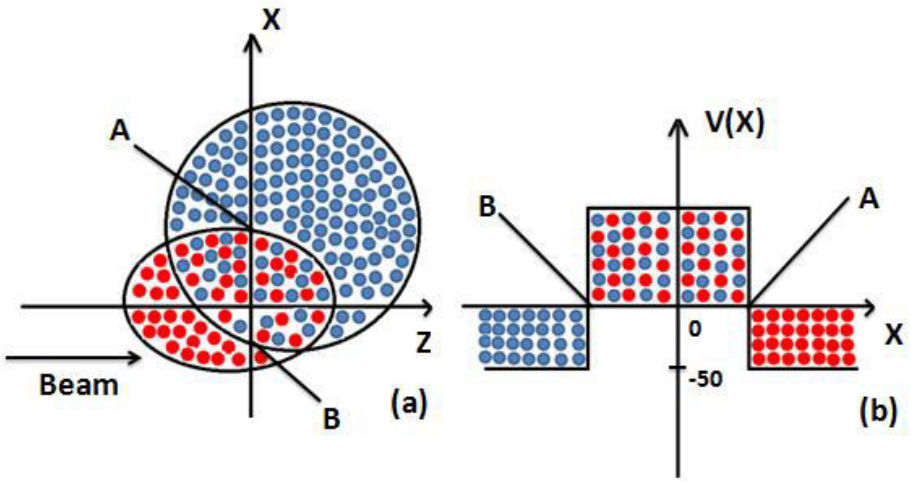

Fig.3.1 The transverse momentum caused by the momentum-dependent forces [8].

The MDI give rise to two new EoS. A set of MDI with soft EoS is called SMD, whereas a hard EoS with MDI is called HMD. There values are given in following table:

EoS	K (MeV)	α (MeV)	β (MeV)	γ	δ (MeV)	ϵ
SMD	200	-390	320	1.14	1.57	21.54
HMD	380	-130	59	2.09	1.57	21.54

It has been seen that, no difference is observed in the soft, hard, SMD and HMD EoS at normal nuclear matter density. On the other hand, the difference between different EoS can be seen with increase in density above normal nuclear matter density. The effect of MDI on the various observables in HICs has been studied for many years [35]. They are also found to affect the multifragmentation and nuclear stopping. This motivated us to study the role of MDI in intermediate energy HICs. However, the inclusion of isospin into the MDIs can give some new fascinating results in nuclear stopping, which is our prime concern. For that, isospin MDI i.e. IMDI is explained in the next section.

3.2 Isospin Momentum Dependent Interactions (IMDI)

Among the various potentials used in IQMD model, given in eq. (7), namely, V_{Skyrme}^{ij}, V_{Yukawa}^{ij} and V_{MDI}^{ij} are isospin independent. The IQMD model [24] has been modified to IQMD (Th01) model [25], by including the isospin degree of freedom in the MDI. With the addition of isospin factor in MDI, we get a new potential which is dubbed as IMDI, such that the total potential now takes the form:

$$V^{ij} = V_{Skyrme}^{ij} + V_{Yukawa}^{ij} + V_{Coul}^{ij} + V_{IMDI}^{ij} + V_{Sym}^{ij} \tag{16}$$

where,
$$V_{IMDI}^{ij} = \left(1.0 - 0.5\, T_3^i T_3^j\right).V_{MDI}^{ij} \tag{17}$$

The above equation implies that, now, MDI behave differently for neutrons and protons. The value 1.0 and 0.5 in the above equation reveals that, the neutron-proton correlations are stronger than that of the neutron-neutron and proton-proton correlations.

Some studies have been reported in the literature that focuses the effect of MDI on nuclear stopping [19]. Although the role of MDI on the dynamical process of the HICs has been studied for many years, little attention has been paid towards the isospin effect of the MDI. Recently, Liu *et al*. [10, 36], considered an isospin degree of freedom in MDI to obtain IMDI. They study the role of IMDI on the isospin fractionation ratio and its dynamical mechanism in the intermediate energy HICs by inserting an isospin degree of freedom into the MDI in IQMD to obtain the IMDI for simulations in IQMD. It is found that the IMDI brings an important isospin effect into the isospin fractionation ratio. Some other authors have also studied the role of IMDI and presented an important isospin effect into the dynamical process involved in the HICs [37]. Ample amount of work has been done to study the various isospin-sensitive observables using IMDI within the framework of IBUU transport model in intermediate energy HICs [38]. Jun Xu *et. al.* [39] gave IMDI in-medium effective interactions for the baryon octet, which is helpful in transport models that simulate HICs in future radioactive beam facilities, particularly at *FAIR/GSI* energies. A formula for IMDI and Skyrme potential for BUU calculations and for HICs induced by neutron-rich nuclei was given by Das Gupta *et al.* [40]. So, from the above review, it would be quite challenging to study the effect of IMDI on various other observables

such as nuclear stopping. The different observables to study the nuclear stopping are discussed in the next section

3.3 Observables to Analyze the Nuclear Stopping

There are several different ways to define the degree of equilibrium.

3.3.1 Anisotropy Ratio

It is an indicator of the global equilibrium of the system. The word 'global' indicates that this quantity does not depend on the local density, and thus, represents the equilibrium of the whole system [17]. It is defined as [10, 23, 41] the ratio of transverse to the longitudinal momentum and is given by:

$$R = \frac{2}{\pi} \frac{(\sum_i |p_\perp(i)|)}{(\sum_i |p_\parallel(i)|)} \tag{18}$$

where, summation runs over all the nucleons. The transverse and longitudinal momenta are $p_\perp(i) = \sqrt{p_x^2(i) + p_y^2}(i)$ and $p_\parallel(i) = p_z(i)$, respectively. For a complete stopping, R should be equal to unity, i.e., there will be uniform distribution of momentum all over the phase space. Stopping is a measure of the efficiency of converting the incoming longitudinal energy of a projectile and target into transverse direction (hence slowing down the incoming nucleons). For the present analysis, the parameter R is used to analyze the degree of stopping for the various simulations carried out.

3.3.2 Quadrupole Moment

Another quantity, which is an indicator of the nuclear stopping, is the quadrupole moment Q_{ZZ}, which is defined as [23, 41]:

$$Q_{ZZ} = \sum_i \left[2p_\parallel^2(i) - p_\perp^2(i)\right] \tag{19}$$

For a complete stopping, Q_{ZZ} should be close to zero. The behavior of $1/Q_{ZZ}$ and R is similar with different parameters.

3.3.3 Rapidity Distribution

We can address the question of equilibrium with the help of rapidity distribution that also shows the stopping of nuclear matter in HICs. It can be defined as [42]:

$$Y(i) = \frac{1}{2}\ln\frac{E(i)+p_{\parallel}(i)c}{E(i)-p_{\parallel}(i)c}, \tag{20}$$

where, *E(i)* and $p_{\parallel}(i)$ are respectively, the energy and longitudinal momentum of the ith particle. A symmetric central collision with a high degree of stopping can be viewed as a thermalized fireball at rest in the centre of mass frame, i.e. at midrapidity. For a complete stopping, one expects a single peaked Gaussian. A narrow Gaussian indicates better thermalization (equilibrium) relative to broader distributions, as, the nuclear stopping is governed by the participant zone only.

3.3.4 Variance (varxz)

This quantity is defined as [11]:

$$varxz = \frac{varx}{varz} = \frac{\sigma^2(x)}{\sigma^2(z)} \tag{21}$$

where, *varx* and *varz* are the variances obtained from the *fwhm* (full width at half maxima) of the rapidity distribution along transverse and longitudinal directions respectively from the relation:

$$fwhm = 2.36 * (varx)^{1/2} \tag{22}$$

More is the value of *varxz*, higher is the stopping achieved, and a value of unity will indicate full stopping.

3.4 Results and Discussions

In the previous chapters, the details of HICs and the different models that are used to analyze them are discussed. For the detailed investigation of IMDI in the nuclear stopping of asymmetric reactions, the simulations have been carried out within the framework of IQMD and IQMD(Th01) models for the various mass asymmetric reactions namely ${}^{16}_{8}O+{}^{197}_{79}Au$, ${}^{32}_{16}S+{}^{197}_{79}Au$,

$^{65}_{30}Zn+^{197}_{79}Au$, $^{118}_{50}Sn+^{197}_{79}Au$, and $^{131}_{54}Xe+^{197}_{79}Au$ at different incident energies and scaled impact parameters, $\hat{b}=b/b_{max}=0,0.3,0.6,0.9$ [where b is particular impact parameter in Fermi (fm) and b_{max} = 1.12 ($A_T^{1/3}$ + $A_P^{1/3}$), A_T and A_P are the masses of target and projectile nuclei respectively] in center of nucleus-nucleus mass frame. A soft EoS has been employed with momentum dependent interactions named SMD and with isospin momentum dependent interactions named as ISMD. The reaction has been carried out till 200 fm/c, which is considered as the freeze-out time. The phase space produced by the IQMD and IQMD (Th01) models has been analyzed with MSTP technique, in which d_{min} is chosen to be 4 fm and p_{min} is chosen to be 150 MeV/c.

3.4.1 Spatial and Momentum Distribution for Mass Symmetric Reactions

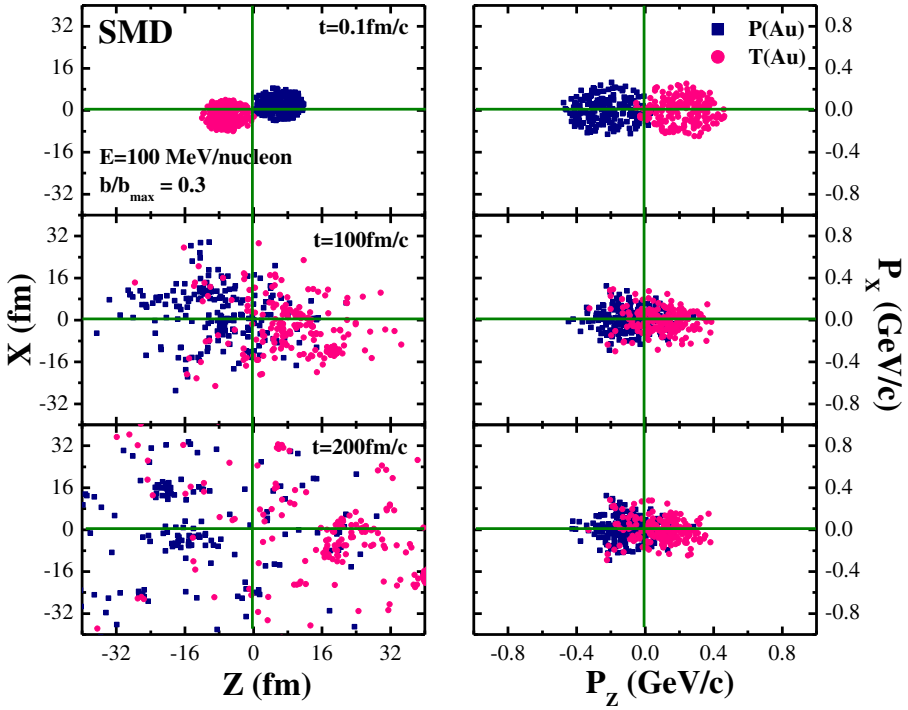

Fig.3.2 Spatial and momentum distribution for mass symmetric reaction $^{197}_{79}Au + {}^{197}_{79}Au$ ***at beam energy E=100 MeV/nucleon and*** $\hat{b}$***=0.3.***

Fig.3.2 shows the spatial and momentum phase space distribution of projectile and target nucleons, in X-Z (left panel) and P_X-P_Z plane (right panel) at an incident beam energy, E=100

MeV/nucleon and scaled impact parameter, $\hat{b}$ = b/b_{max}=0.3, (where $b_{max} = 1.12(A_T^{1/3} + A_P^{1/3})$, in which A_T and A_P are the mass of the target and projectile nuclei respectively, for the case of SMD. The first, second and third row depicts the results for the time steps 0.1 fm/c, 100 fm/c and 200 fm/c respectively. In the case of symmetric reaction, the distribution is appear to be uniform in spatial and momentum space at 200 fm/c, which is due to full stopping or thermalization in this case and the energy is equally transferred to all the nucleons. The target nucleons are drifted in forward direction because of the effect of MDI.

3.4.2 Spatial and Momentum Distribution for Mass Asymmetric Reactions

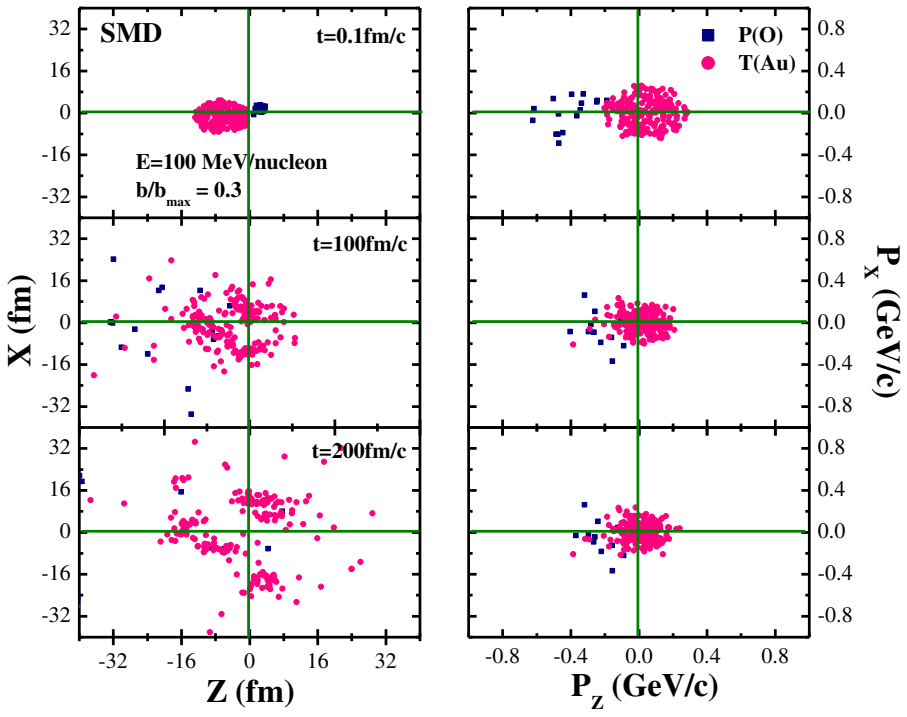

Fig.3.3 Spatial and momentum distribution for mass asymmetric (or lighter projectile) reaction $^{16}_{8}O + {}^{197}_{79}Au$ ***at beam energy E=100 MeV/nucleon and*** $\hat{b}$***=0.3.***

Fig.3.3 shows the spatial and momentum space distribution for same energy and impact parameter as for the previous figure, but for the mass asymmetric (or lighter projectile) reaction $^{16}_{8}O + {}^{197}_{79}Au$. Due to mass asymmetry, the spatial and momentum distribution

becomes non-uniform. This is because the degree of stopping decreases for asymmetric collision due to unequal transfer of energy among the projectile and target nucleons. Also, the preservation of the initial memory of the nucleons is directly related with the number of collision it suffers, so, the momentum space of those nucleons which suffer a large number of collisions is better thermalized. Therefore, the momentum space for asymmetric collision is also non-uniform.

3.4.3 Collision Rate

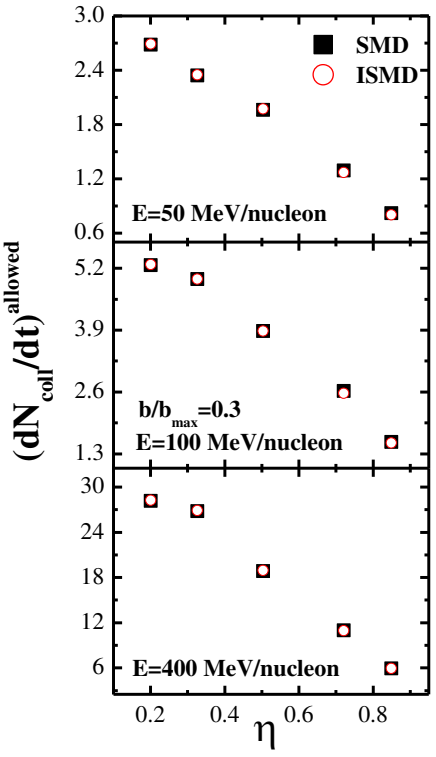

Fig.3.4 Variation of the collision rate with mass asymmetry (η) at E= 50, 100 and 400 MeV/nucleon and $\hat{b}$=0.3. The results with SMD and ISMD are represented by solid square and open circle symbols respectively.

Fig.3.4 represents the variation of the allowed collision rate $(dN_{coll}/dt)^{allowed}$ with mass asymmetry (η) of the reaction at the incident energies 50, 100 and 400 MeV/nucleon and $\hat{b}$=0.3 under the influence of SMD and ISMD. With increase in the mass asymmetry of the reaction, the

collision rate decreases for both SMD and ISMD. This is because as the mass asymmetry increases, the overlapping zone decreases, which reduces the number of collision between the nucleons. So the collision rate decreases. Due to Pauli blocking allowed collision rate for given mass asymmetry is very small. With increase in energy, the collision rate nearly becomes double at 100 MeV/nucleon compared to 50 MeV/nucleon. The role of Pauli blocking is minimum at 100 MeV/nucleon. At higher energies collision dynamics play a significant role i.e. allowed collision rate nearly becomes ten times at 400 MeV/nucleon for any given mass asymmetry.

3.4.4 Variation of the maximum and average density, maximum of total and allowed collision rate with the incident energy

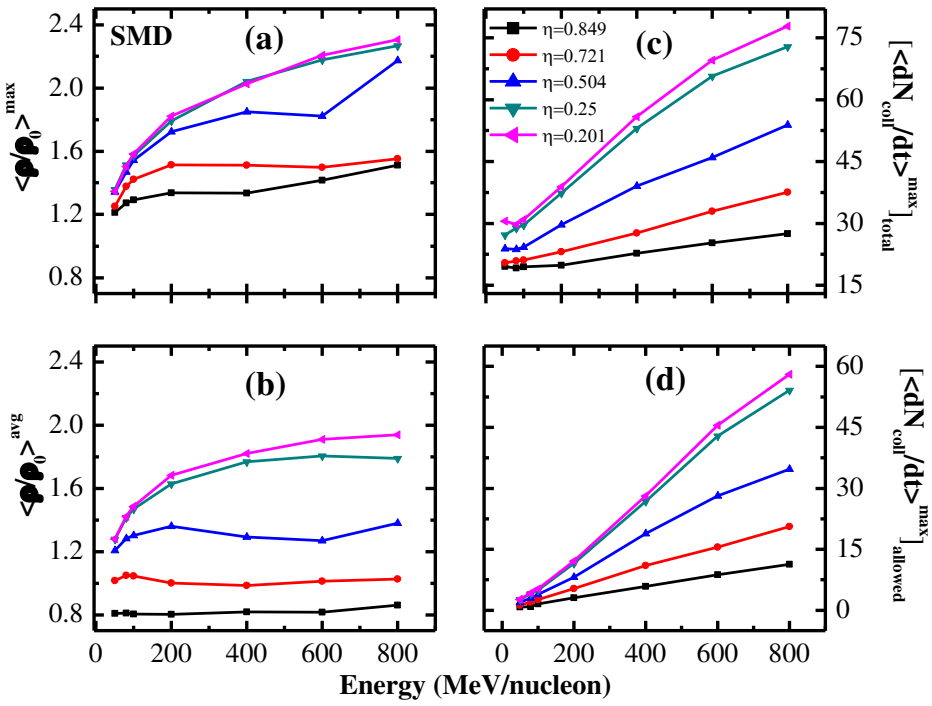

Fig.3.5 Variation of the maximum density ($<\rho/\rho_0>^{max}$), average density ($<\rho/\rho_0>^{avg}$), maximum total collision rate $(<dN_{coll}/dt>^{max})_{total}$ and maximum allowed collision rate $(<dN_{coll}/dt>^{max})_{allowed}$ with incident energy at $\hat{b}$=0.3 for different mass asymmetric reactions under the influence of SMD. Different lines represent the results for different mass asymmetries.

Fig.3.5, shows the variation of the various parameters with incident energy for different mass asymmetric reactions at $\hat{b}$=0.3. Fig.3.5 (a) shows the variation of average maximum density ($<\rho/\rho_0>^{max}$) with incident energy. From the figure, it is clear that with increase in the incident energy $<\rho/\rho_0>^{max}$ increases steeply for nearly heavier projectile reaction, but, as we go towards the mass asymmetry, there is a gradual increase. Similar is the case with the variation of average density ($<\rho/\rho_0>^{avg}$) with incident energy as shown in Fig.3.5 (b). Fig.3.5(c) shows the variation of maximum of the total collision rate [$(<dN_{coll}/dt>^{max})_{total}$] with the incident energy. It indicates the rate of change for collision for both allowed and blocked collisions. Maxima of $(<dN_{coll}/dt>)_{total}$ for different reactions occur at different times. Also, occurs earlier at high energy and later at lower energy which is caused due to the Pauli blocking. It is clear from the Fig.3.5(c), that more the incident energy is pumped into the system, more the maximum density is achieved, and in this highly densed region, more collisions will take place between the nucleons. But, this increase is more for nearly symmetric reactions than for the asymmetric reactions because more will be the number of nucleons, more will be the total energy pumped into the system, so larger will be the number of collisions for symmetric reactions. Fig. 3.5(d) shows the variation of the maximum of allowed collision rate [$(<dN_{coll}/dt>^{max})_{allowed}$] with the incident energy. It indicates the maximum value of the rate of change of allowed collisions only. The trend is similar to that of Fig.3.5(c). Its value also increases with increase in energy but the $(<dN_{coll}/dt>^{max})_{allowed}$ is less than the $(<dN_{coll}/dt>^{max})_{total}$.

3.4.5 Anisotropy ratio of neutron (R_N) and proton (R_P) as a function of incident energy

In order to obtain a clearer picture of the IMDI on nuclear stopping, we display the dependence of the anisotropy ratio for the protons and neutrons separately in Fig.3.6. The figure shows the dependence of the anisotropy (stopping) ratio (R) due to neutrons (R_N) and due to protons (R_P) with incident energy at $\hat{b}$=0.3 for highly asymmetric ($^{16}_{8}O + {}^{197}_{79}Au$) and nearly symmetric ($^{131}_{54}Xe + {}^{197}_{79}Au$) reactions under the influence of SMD and ISMD. The variation between SMD and ISMD can be seen for the asymmetric case. In this case, the stopping first decreases steeply at 100 MeV/nucleon with a dip and then again decreases. The dip occurs because at low

energy, two body collision between the nucleons is greatly suppressed by Pauli blocking and the mean field governs the HIC process and hence, stopping decreases. Then again it increases and finally decreases with energy as at higher energy two body collision plays the dominant role and most of the nucleons suffer violent collisions and get excited to become free, i.e., transparency increases. This trend is not seen in nearly symmetric reactions, where, the stopping decreases gradually with increase in energy.

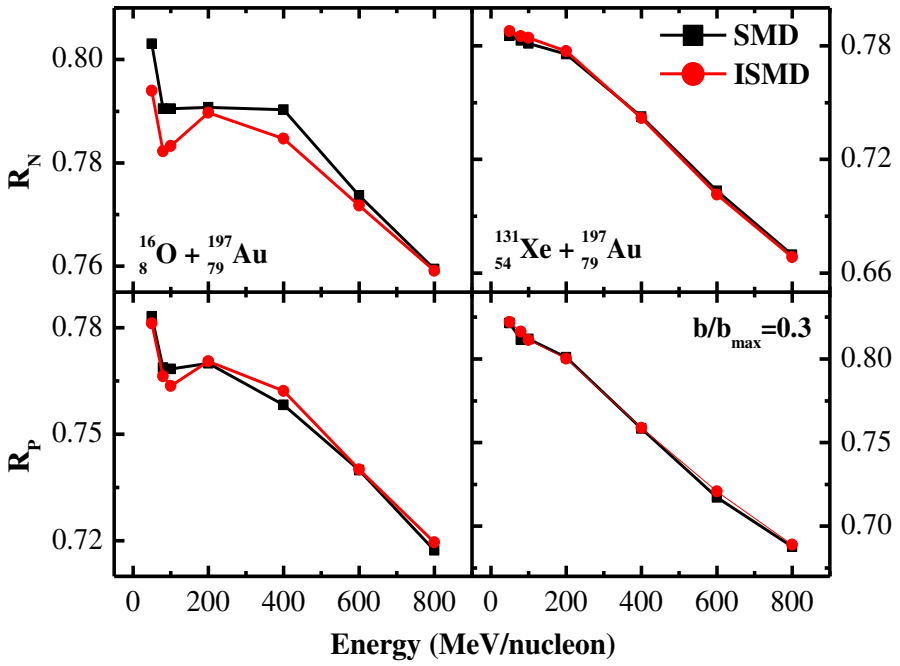

Fig.3.6 Variation of the anisotropy ratio (R) due to neutrons (R_N) and protons (R_P) with incident energy at $\hat{b}$=0.3 for highly asymmetric and nearly symmetric reactions i.e. $^{16}_{8}O + {}^{197}_{79}Au$ and $^{131}_{54}Xe + {}^{197}_{79}Au$ respectively, with SMD and ISMD. Here squared black line and circled red line represent the results for SMD and ISMD respectively.

The MDI decreases the stopping power of the system due to its repulsive nature and an increase in the mean-free path [43]. The difference between SMD and ISMD can be seen for the asymmetric case while no difference can be seen for the case of nearly symmetric reaction. The stopping achieved due to neutrons in case of lighter projectile reaction is larger for SMD, while due to protons, it is larger for ISMD for nearly symmetric systems. This is because the number of protons involved in collision increased considerably. Moreover Coulomb interactions also play

its role. Combined effect of Coulomb interactions and isospin-dependent MDI leads to more stopping.

3.4.6 Anisotropy ratio of neutron and the proton as a function of scaled impact parameter

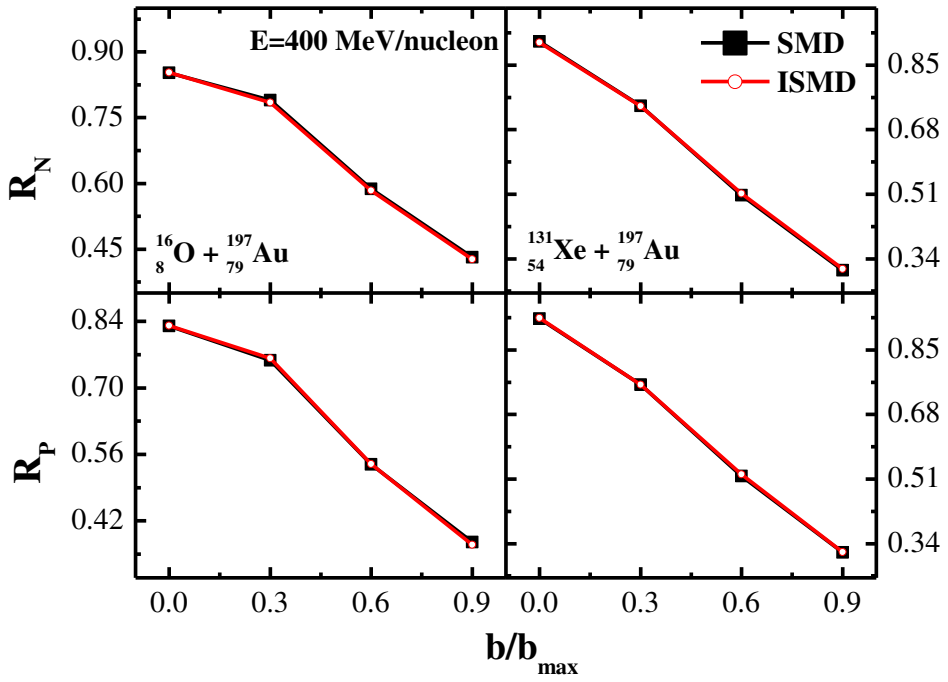

Fig.3.7 Variation of the anisotropic ratio (R) due to neutrons (R_N) and protons (R_P) with $\hat{b}$ for the reactions of $^{16}_{8}O + ^{197}_{79}Au$ and $^{131}_{54}Xe + ^{197}_{79}Au$ at E=400 MeV/nucleon under the influence of SMD and ISMD.

The variation of stopping parameters R_N and R_P with scaled impact parameter for the reactions $^{16}_{8}O + ^{197}_{79}Au$ and $^{131}_{54}Xe + ^{197}_{79}Au$ at E=400 MeV/nucleon is shown in Fig.3.7**.** It can be seen from the figure that with increase in the impact parameter, stopping due to protons and neutrons decreases for lighter projectile as well as heavier projectile reactions. As the impact parameter is increased, the participant zone decreases, while the spectator zone increases, due to which the number of collisions decreases and hence there is lesser thermalization. It is maximum at $\hat{b}$=0 for

both the reacting systems and minimum at $\hat{b}$=0.9. The variation between SMD and ISMD is not visible for both the cases because R is calculated as global phenomena. If we look for stopping in mid-rapidity region, then difference is visible as shown in Fig.3.8. In addition, the figure depicts that the anisotropy ratio is found to be larger in the mid-rapidity region which is caused by the larger contribution of the nuclear stopping in the participant zone as the transverse momentum achieved has maximum strength along the collision zone, i.e. projectile nucleons are stopped by the target nucleon. However, it has been shown in [44], that the nuclear stopping (anisotropy ratio) decreases with the increased contribution of spectator matter, i.e., with increase in the size of rapidity bin.

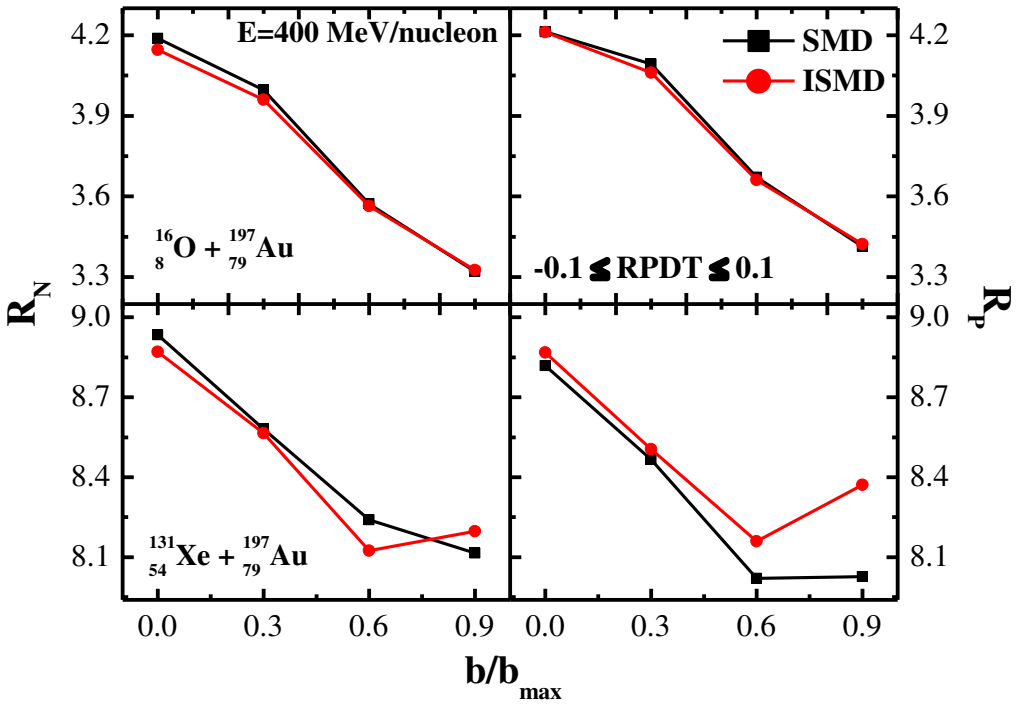

Fig.3.8 Variation of the anisotropic ratio (R) due to neutrons (R_N) (left panels) and protons (R_P) (right panels) with $\hat{b}$ for the reactions of $^{16}_{8}O + ^{197}_{79}Au$ (in upper panel) and $^{131}_{54}Xe + ^{197}_{79}Au$ (in lower panels) at E=400 MeV/nucleon under the influence of SMD and ISMD in the mid-rapidity region.

3.4.7 Anisotropy ratio due to various charged fragments as a function of incident energy

The variation of anisotropy ratio (R) with incident energy for different charged fragments starting from Z=1 up to Z=6 at $\hat{b}$=0.3 for SMD and ISMD is shown in Fig.3.9 for lighter projectile reaction $^{16}_{8}\mathrm{O} + {}^{197}_{79}\mathrm{Au}$. At low energy, heavy fragments are produced which can de-excite themselves by emitting the free nucleons, LCPs and γ rays, thus, increases the isotropy of the system and hence, increases the value of stopping. With increase in energy, stopping first decrease (as very few heavy fragments exist) with a dip, and then decreases for Z=1 and Z=2, as these are produced from participant zone. After 100 MeV/nucleon, stopping increases and reaches saturation for Z= 3, 4, 5, whereas, for the heavier fragment, i.e. Z=6, its value increases.

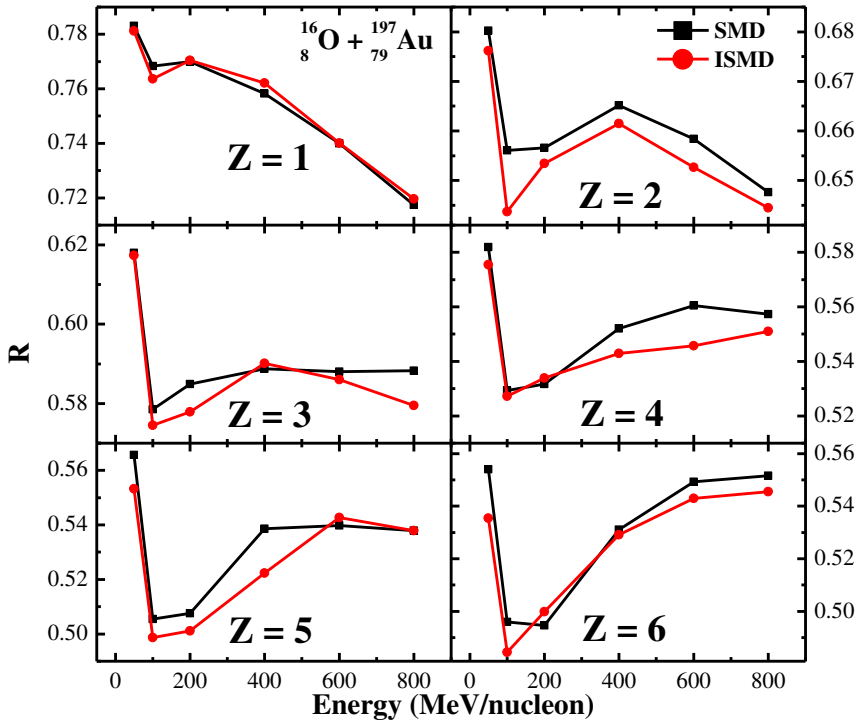

Fig.3.9 Variation of anisotropy ratio (R) with incident energy for different charged fragments at $\hat{b}$=0.3 for the lighter projectile reaction $^{16}_{8}\mathrm{O} + {}^{197}_{79}\mathrm{Au}$ under the influence of SMD and ISMD.

This is due to the fact that fragment production does not change uniformly with increasing charge Z. The contribution of the heavier charged fragments towards stopping is lesser, as these are produced from the spectator part. The variation between SMD and ISMD can be clearly seen from the graphs for all charged fragments. Almost for all the charged fragments, the ISMD has a lesser contribution towards the nuclear stopping. This is due to the reason that, the transfer of the momentum in the transverse direction is lesser with ISMD, which is caused by the lesser density gradient as compared to the SMD. The variation of anisotropy ratio with incident energy for heavier projectile reaction $^{131}_{54}Xe + {}^{197}_{79}Au$ is shown in Fig.3.10 for Z=1 to Z=6. With increase in the incident energy the stopping decreases for all Z, as, at higher energies, the mean free path of the nucleon increases because of the smaller N-N cross section and hence, most of the nucleons will pass through each other, which results in transparency between the projectile and target nucleons. At low energy stopping is more. The difference between SMD and ISMD is not seen for the heavier projectile reaction.

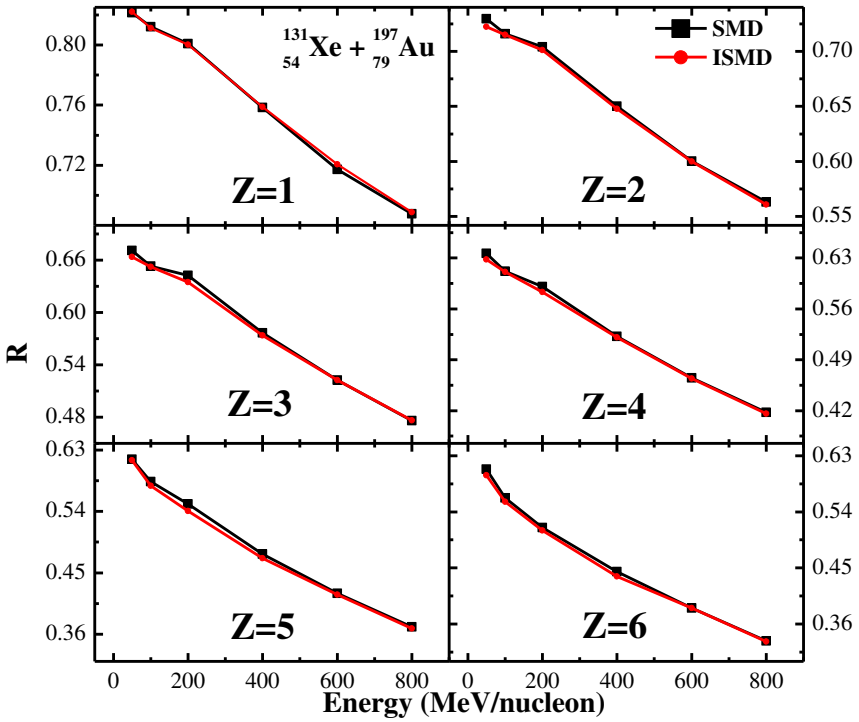

Fig.3.10 Variation of anisotropy ratio (R) with incident energy for different charged fragments at $\hat{b}$=0.3 for the nearly symmetric reaction $^{131}_{54}Xe + {}^{197}_{79}Au$ under the influence of SMD and ISMD.

3.4.8 Dependence of the anisotropy ratio and multiplicity on the fragment charge

Variation of the anisotropy ratio (R) (left panels) and multiplicity (right panels) with charge of fragments at $\hat{b}$=0.3 for the lighter projectile reaction $^{16}_{8}\mathrm{O} + {}^{197}_{79}\mathrm{Au}$ and heavier projectile reaction $^{131}_{54}\mathrm{Xe} + {}^{197}_{79}\mathrm{Au}$ at E=400 MeV/nucleon under the influence of SMD and ISMD is shown in Fig.3.11.

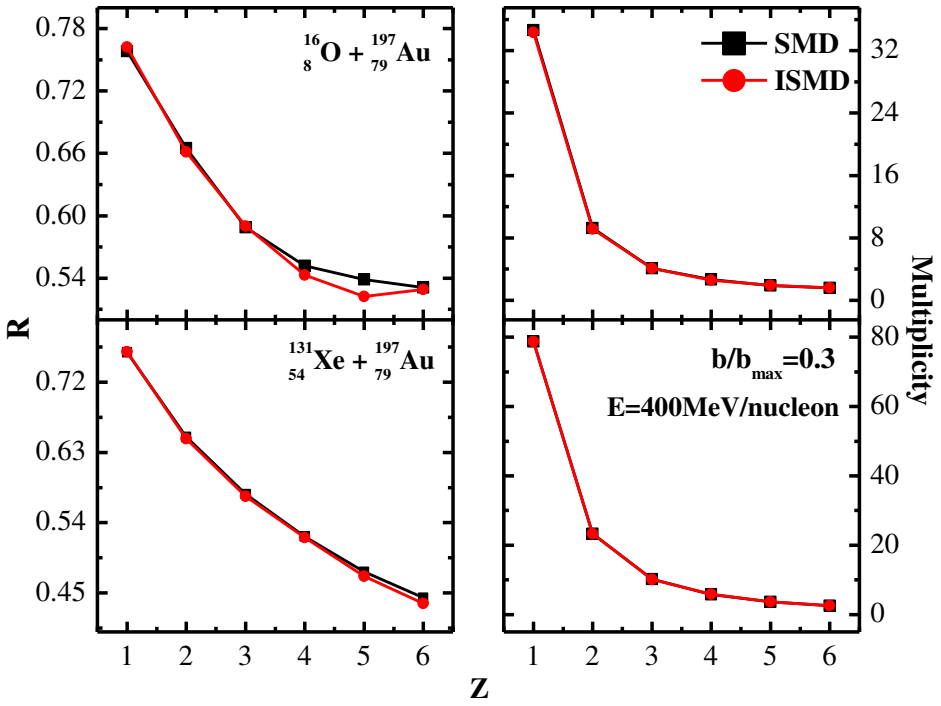

Fig.3.11 Variation of anisotropy ratio (R) and multiplicity with charged fragments at $\hat{b}$=0.3 for the reactions of $^{16}_{8}O + {}^{197}_{79}Au$ and $^{131}_{54}Xe + {}^{197}_{79}Au$ at E=400 MeV/nucleon under the influence of SMD and ISMD.

From the figure, it can be seen that, with increase in the charge of the fragments the stopping decreases. It is because the multiplicity for the higher Z decreases, so lesser is the number of charged particles, lesser will be the value of anisotropy ratio. The sensitivity towards ISMD can be seen in R for higher value of Z, for both the reactions while no difference is seen in multiplicity. This difference in R may be due to the fact that, the higher charged fragments are

produced from the spectator part, for which the MDI and IMDI plays a significant role. For higher Z values, SMD gives larger stopping as compared to the ISMD, because the SMD breaks the spectator part more violently, which gives the large number of higher charged particles, thereby, gives the larger stopping as compared to ISMD. Corresponding to the Fig.3.11, the spatial distribution for different charged fragments of ${}^{16}_{8}O + {}^{197}_{79}Au$ and ${}^{131}_{54}Xe + {}^{197}_{79}Au$, at $\hat{b}$=0.3 and E=400 MeV/nucleon under the influence of SMD and ISMD are shown in Fig.3.11 and Fig.3.12 respectively.

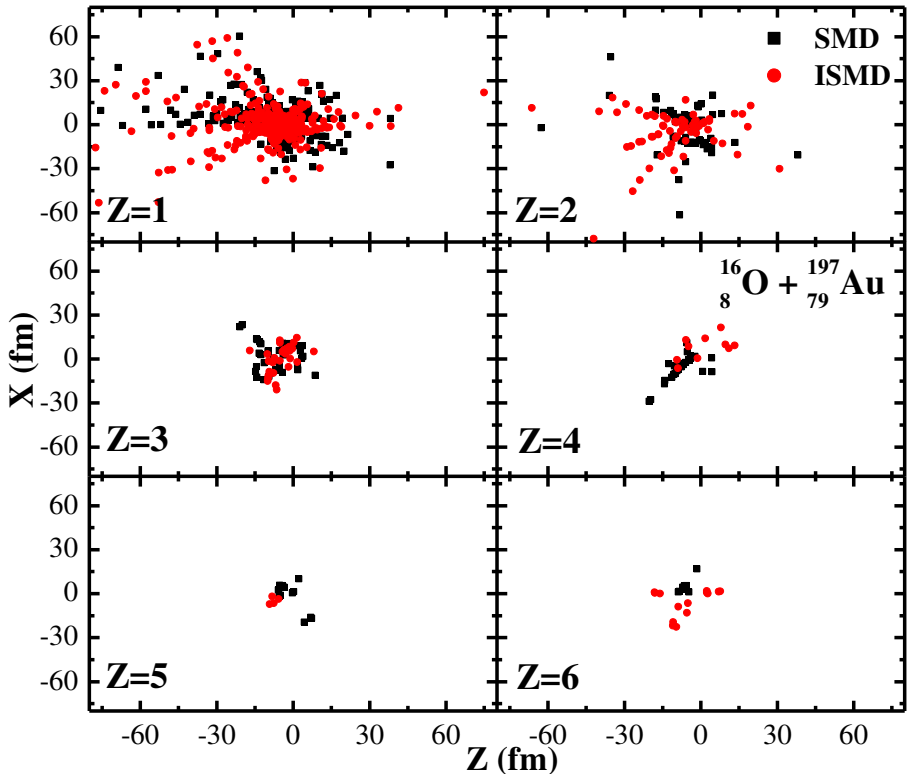

Fig.3.12 Spatial distribution of the lighter projectile reaction ${}^{16}_{8}O + {}^{197}_{79}Au$ ***for different charged fragments at*** $\hat{b}$***=0.3 and E=400 MeV/nucleon under the influence of SMD and ISMD.***

From the figures, it can be seen that the distribution of charged fragments is uniform for heavier projectile (or nearly symmetric) reaction, while it can be seen to be non-uniform for lighter projectile reaction (or mass asymmetric) case around mid-rapidity region. The fragments are seen to move towards the target side in Fig.3.12. The production of heavy charged fragments is lesser as compared to the lighter one for both the reactions. Part of these results has been shown in ref. [45, 46].

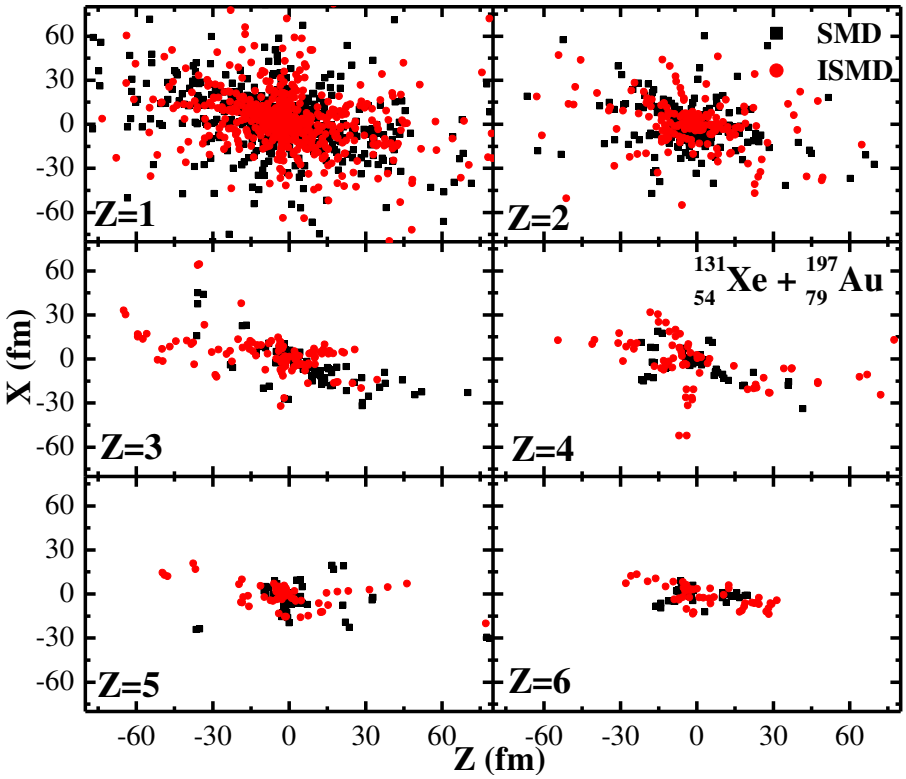

Fig.3.13 Spatial distribution of a heavier projectile reaction $^{131}_{54}Xe + {}^{197}_{79}Au$ *for different charged fragments at* $\hat{b}$*=0.3 and E=400 MeV/nucleon under the influence of SMD and ISMD.*

3.4.9 SUMMARY

In the present work, the nuclear stopping is determined for lighter and heavier projectile reactions with the SMD and ISMD within the framework of respective IQMD and IQMD (Th01) models. It has been revealed that the degree of nuclear stopping decreases for heavier charged fragments, and ISMD plays a significant role in the reactions induced by lighter projectile, whereas negligible role is played for the heavier projectile reaction. Also, if one considers the anisotropy ratio due to neutrons and protons separately, ISMD has been found to play a considerable role for the reaction ${}^{131}_{54}Xe + {}^{197}_{79}Au$ in the mid-rapidity region. This motivates one to further investigate the role of ISMD towards the various aspects of HICs.

REFERENCES

[1]. C.A. Ogilvie *et al.*, Phys. Rev. C **40**, 6 (1989).

[2]. D.C. Tayal, Nuclear Physics, 8th edition, Himalaya Publishing House (2011).

[3]. J. Aichelin and H. Stöcker, Phys. Lett. B **176**, 14 (1986).

[4]. H. Ngo and C.H. Ngo, Nucl. Phys. A **348**, 140 (1980); K.E. Zyromski *et al*., Phys. Rev. C **55**, R 562 (1997).

[5]. B. Jakobsson, Swedish Physical Society **17**, 17053667 (1986).

[6]. S. Kumar, Ph.D Thesis, P.U. Chandigarh (2000).

[7]. X. Campi *et al*., Phys. Rev. C **67**, 044610 (2003).

[8]. J. Aichelin, Phys. Rep. **202**, 233 (1991).

[9]. W. Bauer, Phys. Rev. Lett. **61**, 2534 (1988); B.A. Li, C.M. Ko, Nucl. Phys. A **601**, 457 (1996).

[10]. G. Lehaut *et al*., Phys. Rev. Lett. **104**, 232701 (2010).

[11]. W. Reisdorf *et al*., Nucl. Phys. A **848**, 366 (2010).

[12]. B. Hong *et al*., Phys. Rev. C. **66**, 034901 (2002); F. Rami, Nucl. Phys. A **681**, 309 (2001).

[13]. B. Hong *et al*., Nucl. Phys. A **721**, 317 (2003).

[14]. L. Phair *et al*., Phys. Rev. Lett. **77**, 822 (1996); L.G. Moretto, D.N. Delis and G.J. Wozniak, Phys. Rev. Lett. **71**, 3935 (1993).

[15]. S.A. Bass *et al*., GSI Scientific Report 94 GSI (Germany) 66 (1995).

[16]. B.A. Li, C.M. Ko and W. Bauer, Int. J. Mod. Phys. E **7,** 147 (1998).

[17]. R.K. Puri and A.D. Sood, Heavy Ion Phys. **16**, 429 (2002).

[18]. T. Gaitanos, M. Colonna, M.D. Toro, and H.H. Wolter, Phys. Lett. B **595**, 209 (2004).

[19]. S. Kumar and S. Kumar, Chin. Phys. Lett. **27**, 062504 (2010).

[20]. A.D. Sood and S. Kaur, J. Phys. G **76**, 909 (2011).

[21]. V. Kaur, S. Kumar and R.K. Puri, Nucl. Phys. A **861**, 37 (2011).

[22]. E. Bonnet *et al*., Phys. Rev. C **89**, 034608 (2014).

[23]. S. Kumar, S. Kumar, and R.K. Puri, Phys. Rev. C **81**, 014601 (2010).

[24]. C. Hartnack *et al*., Eur. Phys. J. A **1**, 151 (1998); C. Hartnack *et al*., Phys. Rep. **510**,119 (2012).

[25]. N.K. Virk, K.S. Vinayak and S. Kumar, Proc. DAE Symp. Nucl. Phys. **58**, 310 (2013); K.S.Vinayak, N.K. Virk and S. Kumar, Proc. DAE Symp. Nucl. Phys. **58**, 336 (2013); A. Kaur and S. Kumar, Proc. DAE Symp. Nucl. Phys. **58**, 430 (2013).

[26]. J.P. Bondorf *et al.,* Phys. Rep. **257**, 133 (1995); D.H.E. Gross, Rep. Prog. Phys. **53**, 605 (1990); D.V. Fedorov, A.S. Jensen and E. Garrido, Acta. Phys. Hungarica **18**, 203 (2003).

[27]. H. Stocker and W. Greiner, Phys. Rep. **137**, 277 (1986); A.K. Kerman and S.E. Koonin, Ann. of Phys. **100**, 332 (1976); P. Bonche, S. Koonin and J.W. Negele, Phys. Rev. C **13**, 1226 (1976).

[28]. E.A. Uehling and G.E. Uhlenbeck, Phys. Rev. C **43**, 552 (1933).

[29]. B.A. Li and S.J. Yennello, Phys. Rev. C **52**, R1746 (1995).

[30]. J. Cugnon and C. Volant, Z. Phys. A **334**, 435 (1989).

[31]. R. Bansal *et al.*, Phys. Rev. C **87**, 061602 (2013); S.Kaur and R.K. Puri, Phys. Rev. C **89**, 057603 (2014); S. Kaur and R.K. Puri, Phys. Rev. C **87**, 014620 (2013); E.L. Bratkovskaya *et al.*, Phys. Rev. C **87**, 064907 (2013); S. Gautam *et al.*, J. Phys. G: Nucl. Part. Phys. **37**, 085102 (2010); M. Kaur, V. Kaur and S. Kumar, Phys. Rev. C **88**, 054620 (2013).

[32]. J. Singh, S. Kumar, and R.K. Puri, Phys. Rev. C **62**, 044617 (2000) ; J. Singh and R.K. Puri, *ibid*. **65**, 024602 (2002); R.K. Puri and S. Kumar, *ibid*. **57**, 2744 (1998); S. Kumar and R.K. Puri, *ibid*. **58**, 2858 (1998); S. Kumar, S. Kumar and R.K. Puri*, ibid*. **78**, 064602.

[33]. S. Kumar and R.K. Puri, Phys. Rev. C **58**, 320 (1998); J. Singh and R.K. Puri, *ibid*. **62**, 054602 (2000); S. Kumar, S. Kumar, and R.K. Puri, Phys. Rev. C **81**, 014611 (2010).

[34]. L.G. Arnold *et al.*, Phys. Rev. C **25**, 936 (1982); G. Passatore. Nucl. Phys. A **95**, 694 (1967); G.F. Bertsch and S. Das Gupta, Phys. Rep. **160**, 189 (1988).

[35]. J. Aichelin *et al.*, Phys. Rev. Lett. **58**, 1926 (1987); C. Gale, G.F. Bertsch, and S.D. Gupta, Phys. Rev. C **35**, 1666 (1987); C. Gale *et al*., Phys. Rev. C **41**, 1545 (1990); S. Kumar, S. Kumar and R.K. Puri, Phys. Rev. C **78**, 064602 (2008); J. Singh, S. Kumar and R.K. Puri, Phys. Rev. C **63**, 054603 (2001); S. Gautam and P. Bansal, Phys. Part. Nucl. Lett. **10**, 110 (2013).

[36]. J.Y. Liu *et al*., Chin. Phys. **15**, 1738 (2006).

[37]. J.Y. Liu, W.J. Guo, Y.Z. Xing, and X.G. Lee, Chin. Phys. Lett. **22**, 65 (2005); W.J. Guo and J.Y. Liu, Chin. Phys. C **32**, 172 (2008).

[38]. J. Xu, L.W. Chen, C.M. Ko, and B.A. Li, Phys. Rev. C **81**, 055803 (2010).

[39]. B.A. Li, L.W. Chen and C.M. Ko, Phys. Rep. **464**, 113 (2008); L.W. Chen, C.M. Ko , B.A. Li, and G.C. Yong, Front. Phys. China **2**, 327 (2007).

[40]. C.B. Das, S. Das Gupta, C. Gale and B.A. Li, Phys. Rev. C **67**, 034611 (2003).

[41]. J.Y. Liu *et al.*, Phys. Rev. Lett. **86**, 975 (2001).

[42]. P.B. Gossiaux and J. Aichelin, Phys. Rev. C **56**, 2109 (1997); J.K. Dhawan and R.K. Puri, Phys. Rev. C **75**, 057901 (2007); J.K. Dhawan and R.K. Puri, Phys. Rev. C **74**, 054610 (2006).

[43]. G.Q. Zhang *et al*., Phys. Rev. C **84**, 034612 (2011).

[44]. K.S. Vinayak and S. Kumar, Phys. Ato. Nucl. **76**, 286 (2013).

[45]. N.K. Virk, P. Gautam, and S. Kumar**,** Proc. of 75-years of Nuclear Fission: Present Status and Future Perspectives, May 8-10, 2014, Pg. No. **111**.

[46]. Influence of Isospin Momentum Dependent Interactions on Nuclear Stopping in Mass Asymmetric Nuclear Collisions**,** N.K. Virk, P. Gautam, S. Kumar, R.K. Puri and S. Bhattacharya (to be submitted).